*J. Electrochem. Sci. Eng.* **00(0)** (2022) 000-000; http://dx.doi.org/10.5599/jese.1311

Open Access : : ISSN 1847-9286

www.jESE-online.org

*Original scientific paper*

# Exploration of the effect of Zn-MgO-UPP coating on hardness, corrosion resistance and microstructure properties of mild steel

Itopa Godwin Akande[1,✉], Ojo Sunday Isaac Fayomi[1], Bassey Jonah Akpan[1], Olajide Abraham Aogo[2,3] and Patrick Nwanne Onwordi[1]

[1]*Department of Mechanical Engineering, Bells University of Technology, P.M.B. 1015, Ota, Ogun State, Nigeria*

[2]*Department of Research and Development Unit, Standard Connections Limited, Nigeria*

[3]*Department of Mechanical Engineering, University of Ibadan, Ibadan, Oyo State, Nigeria*

*Corresponding author:* ✉*igakande@bellsuniversity.edu.ng; Tel.: +8035604733*

Received: February 24, 2022; Accepted: April 3, 2022; Published: April xx, 2022

***Abstract***

*This paper investigated the effect of unripe plantain peel (UPP) nanoparticles reinforced Zn-MgO composite coating on the hardness, anti-corrosion and microstructure properties of mild steel. The anti-corrosion characteristics of the coatings were examined using the potentiodynamic polarization method, employing 3.65 % NaCl solution as the test medium. The hardness of the coatings was studied employing the Brinell hardness technique, while the microstructure characteristics were examined using XRD and SEM/EDS. The results of the study revealed that the as-received mild steel sample exhibited the corrosion rate and hardness value of 8.6272 mm year$^{-1}$ and 136.8 kgf mm$^{-2}$, respectively, while the Zn-MgO coated mild steel sample exhibited a corrosion rate and hardness value of 242.5 kgf mm$^{-2}$ and 3.6362 mm year$^{-1}$, respectively. The optimal performing Zn-MgO-UPP coated mild steel sample (sample coated with 20 g L$^{-1}$ of MgO and 6 g L$^{-1}$ of UPP) exhibited a corrosion rate and hardness value of 0.8317 mm year$^{-1}$ and 245.8 kgf mm$^{-2}$, respectively. The corrosion rate and hardness value of the Zn-20MgO-6UPP coated mild steel sample indicated that the UPP nanoparticles further improved the passivating and strengthening ability of Zn-MgO coating. Moreover, the XRD profile of the coatings possessed high intensities, which indicated that the coatings exhibit microstructural and chemical homogeneity, high stability and good texture. It was observed on the SEM micrographs that the Zn-MgO-UPP coating exhibited a more refined microstructure compared to the Zn-MgO coating, indicating the grain refining tendency of the UPP nanoparticles. The EDS further indicated the presence of essential and dispersion strengthening elements in the coatings.*

**Keywords**

SEM; XRD; passivation; composite; homogeneity

## Introduction

The deterioration and operational failure of mild steels have been studied extensively due to their continued relevance in the manufacturing and construction industries [1]. As one of the leading engineering materials, the ready availability and low cost of mild steel have engendered their choice and usage for several engineering applications [2,3]. In spite of the continuous usage of many grades of mild steel, corrosion degradation on exposure to environmental contaminants within a short time of application has reportedly been a challenge [4,5]. It has also been reported that while the corrosion degradation of mild steel occurs rapidly in applications such as petrochemicals, marine and automotive, the corroded segment ultimately exhibits poor microstructure and diminished mechanical properties [6,7], which has led to the failure and total breakdown of structures [8].

Besides failure and total breakdown consequences, corrosion degradation and loss of mechanical properties have resulted in undesired circumstances such as higher maintenance cost, loss and contamination of products, plant shutdown, expensive overdesign and reduction in production efficiency [9,10]. Even though numerous materials have been employed as surface protectors for mild steel, a number of these materials reportedly failed too early, while other seemingly effective materials were regarded inappropriate and toxic to the environment of application [11,12]. For instance, aluminium oxide ($Al_2O_3$) as a protective barrier is limited by its dissolution and instability in a few corrosive media, while titanium oxide ($TiO_2$) has provided more reliable protection due to its chemical stability [13]. However, the improvement of mechanical characteristics and corrosion resistance of mild steel has been accomplished via the combined electrodeposition of $Al_2O_3$ and some metals such as nickel (Ni), zinc (Zn) and copper (Cu) [14,15]. The surface of mild steel and other metals have been successfully coated through the electrodeposition process [16], which has been reported as one of the most broadly used techniques [17].

Coatings produced through the electrodeposition method have also been confirmed durable for metal protection in material engineering over the years [18]. With the aid of electrodeposition certain essential properties have been incorporated into the surface of materials while still retaining their valuable characteristics [19,20]. The deposition of thin film on mild steel through electrodeposition has provided isolation for the metal surface against the surrounded corrosive environments. The thin film may, on occasion, act like galvanized steel where the film oxidizes or corrodes in preference to the metal beneath [21-23]. More so, environment-friendly materials such as by-products of fruit and agricultural wastes have been incorporated into some alloys for their reinforcement. For instance, included in Al6063 were nanosized carbonized chicken bone particles to enhance its microstructural characteristics, corrosion resistance and mechanical properties [24]. Moreover, concrete was strengthened using unripe plantain peel ash. The strengthening effect of the ash could be ascribed to the existence of compounds such as $Al_2O_3$, CaO, $SiO_2$, $Fe_2O_3$ and MgO in the ash [25]. In this present research, unripe plantain peel (UPP) particles were added to Zn-MgO coating, and the effect of UPP on the corrosion, hardness and microstructural properties of Zn-MgO coating were examined. The effect of Zn-MgO-UPP coating on the properties of mild steel was also investigated. The UPP nanoparticles were included with the aim of enhancing the eco-friendliness of the coating.

## Experimental

### *Source of mild steel and deposit materials*

Table 1 indicates the percentage weight of constituents in the mild steel plate used, procured in Ogun State, Nigeria. The chemical composition of the mild steel was determined using an X-ray

fluorescence spectroscopy, through which 99.145 % iron was observed. The major deposit material (zinc bar) was also purchased in Nigeria, Ogun State. The zinc bar was also observed to contain 99.5 % zinc. Moreover, the other deposit materials, such as the nano-size unripe plantain peel (UPP), magnesium oxide (MgO) and reagents, were likewise sourced in Ogun State.

***Table 1.*** *Composition of constituents in the mild steel used*

| Element | C | Si | S | Ni | Mn | Al | P | Fe |
|---|---|---|---|---|---|---|---|---|
| Content, wt. % | 0.152 | 0.184 | 0.032 | 0.006 | 0.461 | 0.008 | 0.012 | 99.145 |

*Preparation of materials prior to coating*

The as-received mild steel plate was cut to samples of dimension 60 × 30 × 2 mm and polished with emery papers of different grades to remove corrosive scales and oxide layers on the surface of the samples. The zinc bars (anodes) of dimension 80×40×20 mm were also rinsed in distilled water and cleaned to get rid of some surface impurities. The UPP nanoparticles were produced from unripe plantain peels. The peels were dried and ground to a nano-size form of about 25 µm. The surfaces of the polished mild steel samples were cleaned by immersion in 0.01 M $Na_2CO_3$ for 10 s and pickled in 10 % HCl at room temperature of 25.4 °C for 10 s in preparation for the electrodeposition.

*Preparation of coating bath*

Four coating baths were prepared in beakers containing 1000 litres of deionized water after a preliminary run of experiments. The weighed particles and reagents were poured into the beakers and stirred vigorously to dissolve. For the Zn-MgO-UPP baths, the mass concentration of MgO was held constant at 20 g $L^{-1}$, while the concentration of the UPP nanoparticles was varied (2, 4 and 6 g $L^{-1}$). The Zn-MgO bath was prepared without UPP nanoparticles. Table 2 shows the bath formulation for the coatings.

***Table 2.*** *Bath composition of the coatings*

| Coating bath constituents | Mass concentration, g $L^{-1}$ |
|---|---|
| ZnO | 20 |
| UPP | 0,2,4,6 |
| Boric acid | 10 |
| Thiourea | 10 |
| $Na_2SO_4$ | 5 |
| $K_2SO_4$ | 5 |
| $ZnSO_4$ | 15 |
| $MgSO_4$ | 20 |
| ZnCl | 20 |

*Electrodeposition process*

The coating of the steel samples through electrodeposition was accomplished in accordance with the ASTM A53M standard. Before the initiation of the coating, the developed bath was heated to 45 °C and kept constant. The zinc anodes were inserted in the bath 5 cm apart and connected to the positive terminal of the rectifier, while a mild steel sample (cathode) was connected to the negative terminal of the rectifier. The electrolyte in the bath was stirred constantly at the rate of 200 rpm during the deposition process to reduce the particle agglomeration and aid the particles electrophoresis (migration of ions to the cathode). The deposition was achieved at the current density of 1.5 A $cm^{-2}$, a voltage of 2.5 V and a time of 20 minutes. Table 3 indicates the process parameters employed for the

deposition, which were arrived at after some preliminary experimental runs. The coatings developed, whose cross-sections are shown in Figure 1, were thereafter dried in natural air and sectioned to 15×10×2 mm for the desired characterizations. The nomenclatures of the coated steels are as follows: Zn-20MgO (Zinc deposit with 20 g of magnesium oxide), Zn-20MgO-2UPP (Zinc deposit with 20 g of magnesium oxide and 2 g of unripe plantain peel particles), Zn-20MgO-4UPP (Zinc deposit with 20 g of magnesium oxide and 4 g of unripe plantain peel particles) and Zn-20MgO-6UPP2UPP (Zinc deposit with 20 g of magnesium oxide and 6 g of unripe plantain peel particles).

***Figure 1.*** *Cross-sections of coated samples*

***Table 3.*** *Process parameters of deposition*

| Parameters | Value |
|---|---|
| pH | 4.8 |
| Cell voltage, V | 2.5 |
| Current density, A $cm^{-2}$ | 1.5 |
| Time, min | 20 |
| Stirring rate, rpm | 200 |
| Temperature, $^{o}C$ | 45 |

*Characterization of samples*

The thickness of the developed coatings was examined using a mini thickness gauge with ± 0.05 accuracy. The thickness of each coating was examined in three different portions on the samples, and the average thickness was calculated. The corrosion properties of the coatings were investigated in a three-electrode system (reference, counter and working electrodes) containing simulated seawater (3.65 % NaCl solution) following the ASTM G102 standard. The reference electrode is the silver/silver chloride, the counter electrode is a graphite rod, while the working electrode is the uncoated or the coated steel sample embedded in epoxy. Using an Auto lab PGSTAT 101 and a computer system on which NOVA 2.1.2 software was installed, the polarization curves were generated at a scan rate of 0.005 V $s^{-1}$, between -1.5 and 1.5 V versus the open circuit potential (OCP) for 1 hour at a room temperature of 25.3 $^{o}C$. The corrosion rate and polarization resistance of the samples were estimated using Eqs. (1) and (2), respectively.

$$CR = \frac{0.00327 j_{corr} w_{eq}}{\rho} \quad (1)$$

$$PR = \frac{2.303 b_a b_c}{j_{corr}(b_a + b_c)} \quad (2)$$

where $\rho$ / g $cm^{-3}$ is the density of the material, $w_{eq}$ / g is the equivalent weight of the and $j_{corr}$ is the corrosion current density. The corrosion rate values were obtained in mm $year^{-1}$.

Moreover, the microstructure of the coatings was studied using XRD (Rigaku D/Max-lllC model) and SEM/EDS (JOEL JSM-7600F model), while the hardness of the as-received and coated samples was examined in accordance with ASTM A833 standard using the Eseway DVRB-M modelled Brinell hardness machine. This hardness measuring machine has a load-bearing capacity ranging from 2.5 to 187.5 kgf. The test samples were subjected to a load ($P$) of 30 kgf for 30 seconds using a hardened indenting steel ball of diameter ($D$ = 10 mm). The indentations diameter ($d$) was measured with a mini microscope. The Brinell hardness values of the materials were then evaluated using Eq. (3).

$$BHV = \frac{2P}{\pi D\left(D - \sqrt{D^2 - d^2}\right)} \quad (3)$$

## Results and discussion

*Weight gained by samples and thickness of the coatings*

Table 4 shows the weight gained by the coated samples. The Zn-20MgO coating was observed to possess the largest weight gain of 0.38 g, while the Zn-20MgO-2UPP coating exhibited the least. Similarly, the coating thickness of the samples indicated in Figure 2 conforms to the weight gained. The Zn-20MgO coating was observed to possess the largest thickness of 389.5 µm, while the Zn-20MgO-2UPP coating exhibited the least thickness of 113 µm. Though, the thickness of coatings could influence their stability [26].

***Table 4.*** *Weight gained by the coated samples*

| Sample | Weight before coating, g | Weight after coating, g | Weight gained, g |
|---|---|---|---|
| As-received | 29.93 | - | - |
| Zn-20MgO | 30.03 | 30.41 | 0.38 |
| Zn-20MgO-2UPP | 29.49 | 29.56 | 0.07 |
| Zn-20MgO-4UPP | 29.52 | 29.68 | 0.16 |
| Zn-20MgO-6UPP | 29.63 | 29.72 | 0.09 |

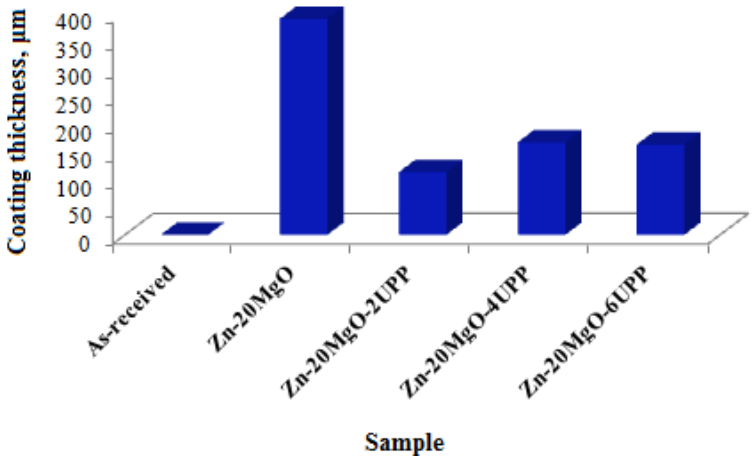


***Figure 2****. Thickness of the coatings*

Coating thickness could sometimes be proportional to the adhesive strength and other outstanding coating properties [27]. However, the thickest coating might, in some cases, not be the best coating due to the probable existence of internal defects or microvoids [28]. The notably low thickness possessed by the Zn-MgO-UPP coatings could be that the UPP nanoparticles hindered the growth of the grains in the coated matrix, thus producing thin films of good quality, as asserted by M. Islam *et al.* [29].

*Corrosion characteristics of the as-received and coated samples*

Table 5 and Figure 3 show the polarization date and polarization curves, respectively. The Zn-20MgO coated sample exhibited better corrosion resistance than the as-received. While the as-received sample possessed the corrosion rate (*CR*) of 8.6272 mm year$^{-1}$, corrosion current density, $j_{corr}$ of 0.74245 mA cm$^{-2}$ and polarization resistance (*PR*) of 86.45 Ω, the Zn-20MgO coated sample exhibited a lower CR of 3.6362 mm year$^{-1}$, low $j_{corr}$ of 0.31293 mA cm$^{-2}$ and high PR of 195.98 Ω. This indicated the Zn-20MgO coated sample provided an inhibitive effect against the entrance of the NaCl solution into the active sites of the steel [30,31]. The Zn-MgO-UPP coatings were observed to exhibit superior corrosion resistance compared to the Zn-20MgO coatings. Relative to the entire samples, the Zn-20MgO-6UPP coated sample exhibited the lowest *CR* and $j_{corr}$ of 0.8317 mm year$^{-1}$ and 0.071578 mA cm$^{-2}$, respectively. This indicated that the Zn-20MgO-6UPP coating provided the best corrosion resistance against the dilapidating effect of the corrosive ions from the 3.65 % NaCl solution. The reason for this could be the doping effect of the UPP nanoparticles, filling the nano-holes in MgO coating and providing supportive covering against the diffusion of the chloride to the anodic and cathodic sites of the steel [32,33].

***Table 5.*** *Polarization data for the as-received and coated samples*

| Sample | $E_{corr}$ / V | $j_{corr}$ / mA cm$^{-2}$ | *CR* / mm year$^{-1}$ | *PR* / Ω |
|---|---|---|---|---|
| As-received | -0.7991 | 0.742 | 8.6272 | 86.45 |
| Zn-20MgO | -0.6785 | 0.313 | 3.6362 | 195.98 |
| Zn-20MgO-2UPP | -0.7986 | 0.187 | 2.1742 | 198.9 |
| Zn-20MgO-4UPP | -1.3235 | 0.106 | 1.2344 | 274.51 |
| Zn-20MgO-6UPP | -0.7994 | 0.072 | 0.8317 | 712.91 |

Moreover, Figure 3 further indicated that the Zn-MgO coating acted predominantly as an anodic corrosion protective coating, while the Zn-20MgO-2UPP and Zn-20MgO-6UPP coatings acted predominantly as a mixed-type inhibitor or mixed corrosion protective coating [34].

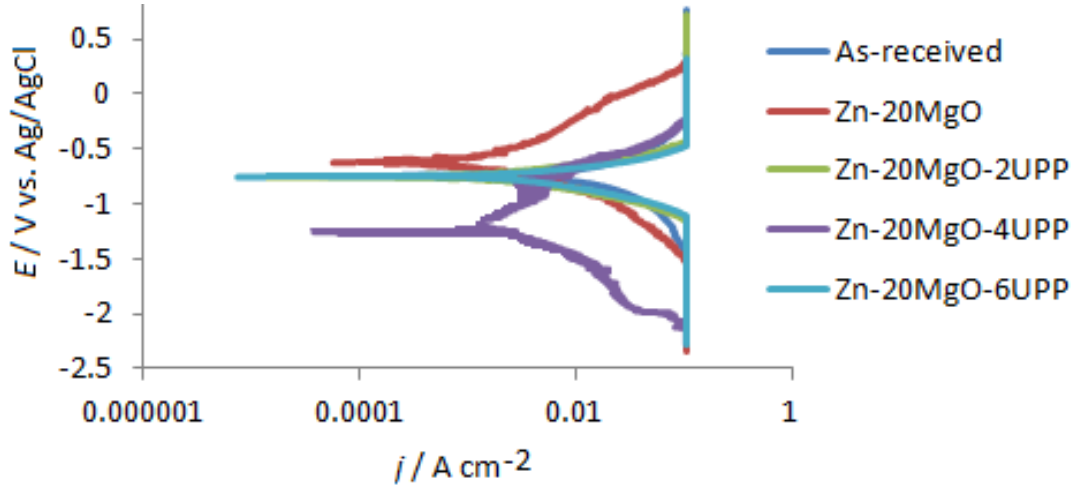


***Figure 3.*** *Polarization curve for the as-received and coated samples*

However, the Zn-20MgO-4UPP coating behaved predominantly as cathodic corrosion protective coating, as revealed by the negative shift in its polarization curves with respect to those of the as-received sample [35]. Also, Figure 4 shows the OCP versus time curves of the samples, which indicated that the samples exhibited stable state potentials between 40 and 120 seconds of immersion [36].

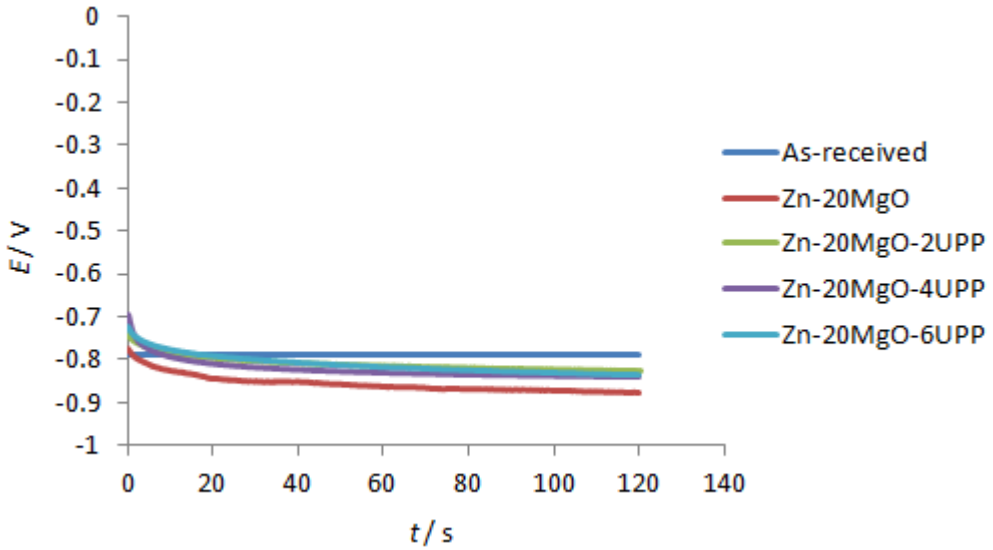


***Figure 4.*** *Open circuit potential for the as-received and coated samples*

*Microstructure properties of the coatings*

Some microstructural properties of the Zn-20MgO and Zn-20MgO-6UPP coated steel are shown in Figure 5-Figure 8. The SEM image of the Zn-20MgO coated sample in Figure 5 revealed that the sample exhibited refined surface morphology. The coated surface was observed flake-like structure with few cavities. Conversely, the SEM image of the Zn-20MgO-6UPP coated sample in Figure 6 exhibited more refined grains with nodule structure. The grains and grain boundaries observed on the surface of the Zn-20MgO-6UPP coated sample were smaller than those on the Zn-20MgO coated sample. This could have been the reason for the better corrosion resistance characteristics of the Zn-20MgO-6UPP coated sample. Thus, the small grains and grain boundaries could have prevented the possibility of the grain boundaries to act as crevices for attack by corrosives [37,38]. Therefore, from the examination of SEM image of the Zn-20MgO coated sample, it is expected to exhibit inferior mechanical and corrosion resistance characteristics compared to the Zn-20MgO-6UPP coated sample since microstructure behaviour of materials affects other major properties such as mechanical, corrosion and thermal resistance properties [39]. This shows the unripe plantain peel (UPP) particles exhibit grain refining characteristics. More so, the EDS of the Zn-20MgO coated sample in Figure 5 revealed elements such as C, Si, O, Mg, Na and Fe. However, the EDS of the Zn-20MgO-6UPP coating revealed a larger percentage weight of carbon (C) compared to the carbon content in the Zn-20MgO coating. Calcium (Ca) was also revealed to be present on the surface of the Zn-20MgO-6UPP coating, which is not found on the Zn-20MgO coating. The larger percentage weight of carbon and the Ca in Zn-20MgO-6UPP coating could have been deposited from the unripe plantain peel (UPP) particles.

Furthermore, the XRD profile of the Zn-20MgO and Zn-20MgO-6UPP coated steel shown in Figures 7 and 8, respectively, indicated the predominant crystallographic phases in both coatings are MgO, FeO and SiO. The highest peak intensity phase in the Zn-20MgO coating is the crystal of MgO, which was observed at the intensity of 510 a.u ($2\theta$ is about 26°). In the Zn-20MgO-6UPP coating, the highest peak intensity phase (a crystal of MgO) was lower; at the intensity of 490 a.u. ($2\theta$ is about 42°). Although it has been reported that the higher the peak intensity of phases in a coating, the more the stability of the coating and the less the microstructure lattice defects [40]. However, there are indications that the UPP nanoparticles could probably have suppressed the growth of MgO in the matrix of Zn-20MgO-6UPP coating to refine the grains [41-43]. Hence, the

peak could also contain some out of sight elements that are not captured with the crystal. More so, the Zn-20MgO-6UPP coating also has a fairly high peak intensity of $MgSiO_2$, $MgFeO_2$ and $FeSiO_2$ crystallographic phases, which could be beneficial to the mechanical and corrosion-resistant properties of the coating. These high peak intensities revealed that the coatings exhibited microstructural and chemical homogeneity, good texture and high stability [44].

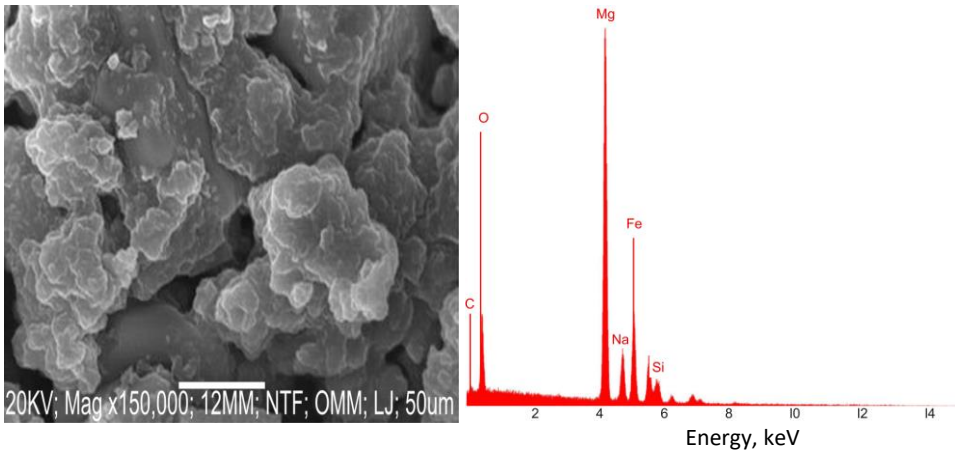


***Figure 5.*** *SEM/EDS images of Zn-20MgO coated steel*

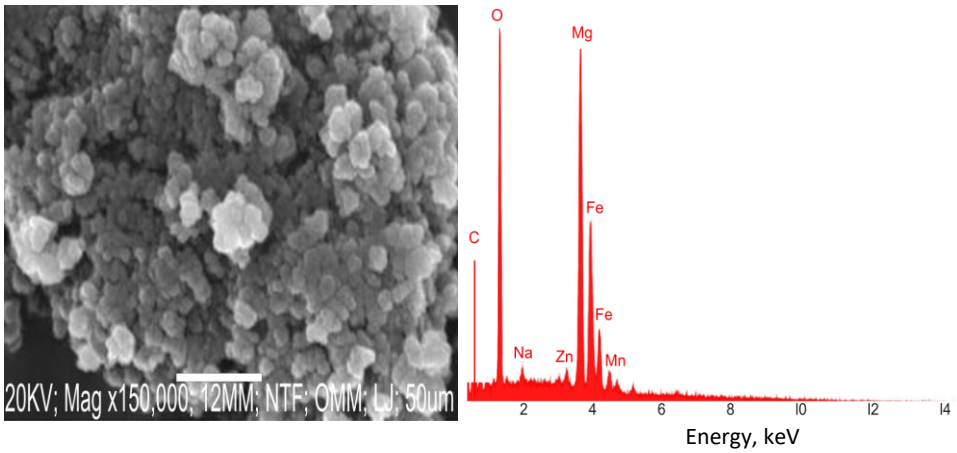


***Figure 6.*** *SEM/EDS images of Zn-20MgO-6UPP coated steel*

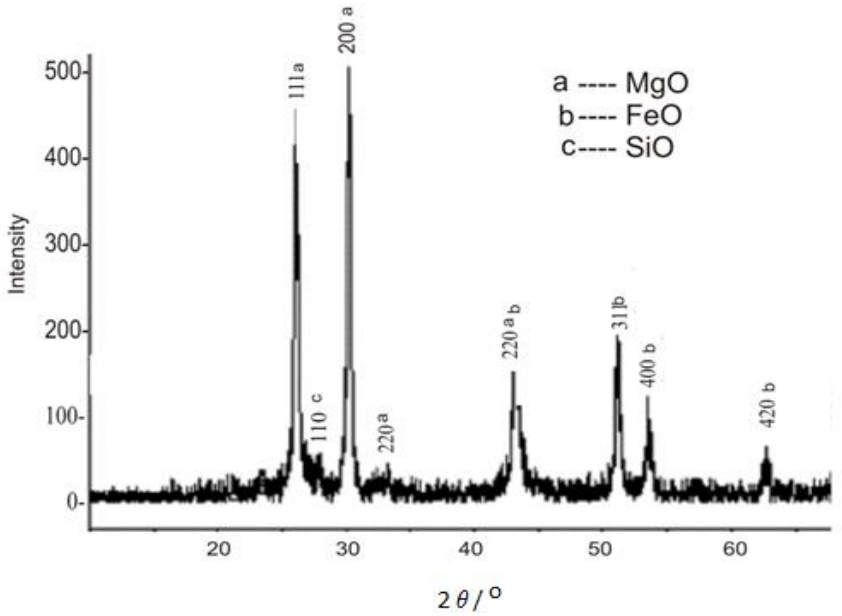


***Figure 7.*** *XRD profile of Zn-20MgO coated steel*

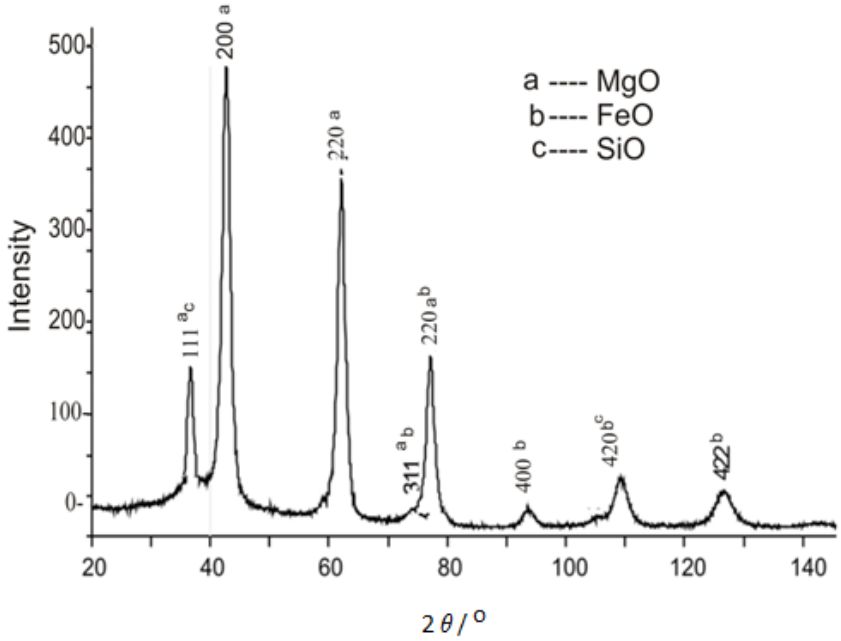


***Figure 8.*** *XRD profile of Zn-20MgO-6UPP coated steel*

*Brinell hardness of samples*

The Brinell hardness of the as-received and coated samples is shown in Figure 9. The coated samples exhibited notably high hardness values compared to the as-received samples. This shows that the coatings adhered firmly to the mild steel [45]. The strong adhesion could have resulted from the right choice of the process parameters, such as temperature, which aids the total dissolution of the coating constituents to form formidable layers at the steel-coating interface [46,47]. However, the entire Zn-MgO-UPP coated steel exhibited superior hardness to the MgO coated steel. This indicated that the UPP (unripe plantain peel) nanoparticles provided some grain boundaries strengthening effect, minimizing slip and dislocation of the grains contained in the coatings [48,49]. While the as-received sample exhibited the least hardness of 136.8 kgf $mm^{-2}$, the Zn-20MgO-6UPP coated sample exhibited the highest hardness value of 245.8 kgf $mm^{-2}$. This signified that the Zn-20MgO-6UPP coating provided the most impervious laminating covering against the indenting force. Moreover, the high UPP nanoparticles could also have significantly reinforced the grain boundaries against slip and dislocation of the grains, thus strengthening the coating appreciably [50].

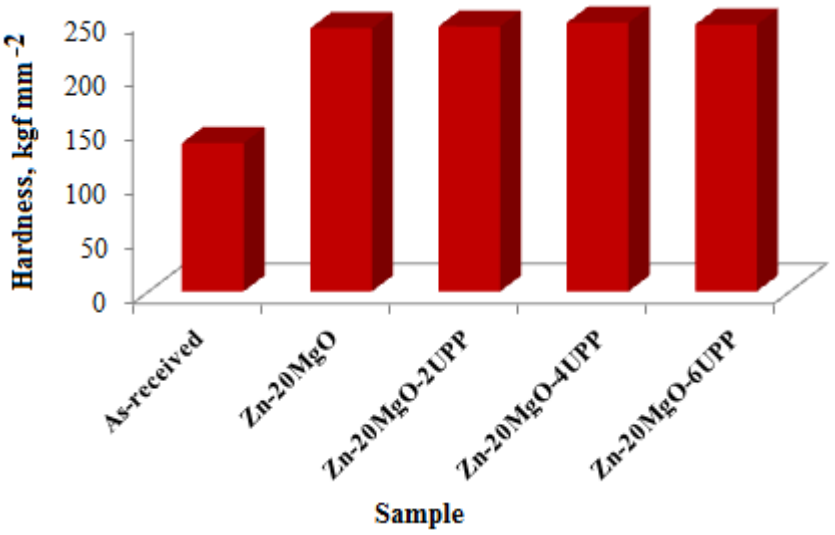


***Figure 9.*** *Hardness of the as-received and coated samples*

## Conclusions

i) From this work, the Zn-MgO coating was observed to exhibit the highest thickness compared to the other coatings. The thickness of the Zn-MgO coating was 389.5 µm.

ii) More so, the uncoated mild steel sample exhibited the hardness value and corrosion rate of 136.8 kgf $mm^{-2}$ and 8.6272 mm $year^{-1}$, respectively, while the Zn-MgO coated mild steel exhibited hardness and corrosion rate of 242.5 kgf $mm^{-2}$ and 3.6362 mm $year^{-1}$, respectively. This indicated that the Zn-MgO coating strengthened the steel to some level and also offered some passivating effects in the test medium.

iii) The optimal performing Zn-MgO-UPP coated steel (sample coated with 20 g $L^{-1}$ of MgO and 6 g $L^{-1}$ UPP) exhibited the hardness and corrosion rate of 245.8 kgf $mm^{-2}$ and 0.8317 mm $year^{-1}$, respectively. This indicated that the UPP particles further strengthened the Zn-MgO coating, and also enhanced the passivating ability of the coating.

iv) Furthermore, the SEM micrographs indicated that the Zn-MgO-UPP coating exhibited a more refined microstructure compared to the Zn-MgO coating. This shows that the UPP nanoparticles exhibited a grain refining tendency. The XRD profile of the coatings also indicated the coatings exhibited high peak intensities. The high peak intensity of MgO and FeO phases and fairly high peak intensity of $MgSiO_2$, $MgFeO_2$ and $FeSiO_2$ phases revealed that the coatings exhibited microstructural and chemical homogeneity, good texture and high stability.

## References

[1] E. Ohaeri, U. Eduok, J. Szpunar, *International Journal of Hydrogen Energy* **43** (2018) 14584-14617. https://doi.org/10.1016/j.ijhydene.2018.06.064

[2] M. Shivakumar, M. S. Dharmaprakash, S. Manjappa, K. L. Nagashree, *Portugaliae Electrochimica Acta* **35** (2017) 351-359. http://dx.doi.org/10.4152/pea.201706351

[3] M. Murmu, S. K. Saha, N. C. Murmu, P. Banerjee, *Journal of Molecular Liquids* **278** (2019) 521-535. https://doi.org/10.1016/j.molliq.2019.01.066

[4] O. S. I. Fayomi, I. G. Akande, D. E. Ighravwe, D. O. Aikhuele, *Key Engineering Materials* **886** (2021) 119-125. https://doi.org/10.4028/www.scientific.net/KEM.886.119

[5] R. A. Rahman Rashid, M. A. Javed, C. Barr, S. Palanisamy, N. Matthews, M. S. Dargusch, *International Journal of Advanced Manufacturing Technology* **117** (2021) 2949-2958. https:/doi.org/10.1007/s00170-021-07886-7

[6] W. Wu, Q. Wang, L. Yang, Z. Liu, X. Li, Y. Li, *Journal of Materials Research and Technology* **9** (2020) 12976-12995. https://doi.org/10.1016/j.jmrt.2020.09.033

[7] T. O. Olugbade, *Analytical Letters* **54** (2021) 1055-1067. https://doi.org/10.1080/00032719.2020.1793994

[8] R. Wang, R. A. Shenoi, A. Sobey, *Journal of Constructional Steel Research* **143** (2018) 331-342. https://doi.org/10.1016/j.jcsr.2018.01.014

[9] J. C. Kurth, P. D. Krauss, S. W. Foster, *Transportation Research Record* **2673** (2019) 2-14. https://doi.org/10.1177/0361198119855333

[10] O. S. I. Fayomi, I. G. Akande, C. Ofo*, Key Engineering Materials* **886** (2021) 159-167. https://doi.org/10.4028/www.scientific.net/KEM.886.159

[11] G. Bahlakeh, B. Ramezanzadeh, M. Ramezanzadeh, *Journal of Cleaner Production* **210** (2019) 872-886. https://doi.org/10.1016/j.jclepro.2018.11.089

[12] A. Arul, S. Sivagnanam, A. Dey, O. Mukherjee, S. Ghosh, P. Das, *RSC Advances* **10** (2020) 13420-13429. https://doi.org/10.1039/C9RA10018K

[13] M. A. Fusco, C. J. Oldham, G. N. Parsons, *Materials* **12** (2019) 672. https://doi.org/10.3390/ma12040672

[14] M. Shourgeshty, M. Aliofkhazraei, A. Karimzadeh, *Surface Engineering* **35** (2019) 167-176. https://doi.org/10.1080/02670844.2018.1432172
[15] M. Alizadeh, H. Safaei, *Applied Surface Science* **456** (2018) 195-203. https://doi.org/10.1016/j.apsusc.2018.06.095
[16] O. S. I. Fayomi, G. A. Oluwadare, O. B. Fakehinde, I. G. Akande, W. Nwachia, U. Oziegbe, A. J. Russell, *International Journal of Advanced Manufacturing Technology* **103** (2019) 2621-2625. https://doi.org/10.1007/s00170-019-03714-1
[17] A. Lelevic, F. C. Walsh, *Surface and Coatings Technology* **369** (2019) 198-220. https://doi.org/10.1016/j.surfcoat.2019.03.055
[18] R. Manivannan, S. N. Victoria, *Solar Energy* **173** (2018) 1144-1157. https://doi.org/10.1016/j.solener.2018.08.057
[19] A. D. Torkamani, M. Velashjerdi, A. Abbas, M. Bolourchi, P. Maji, *Journal of Composites and Compounds* **3** (2021) 106-113. https://doi.org/10.52547/jcc.3.2.4
[20] R. Bhat, A. C. Hegde, *J. Electrochem. Sci. Eng.* **9(1)** (2019) 9-16. https://doi.org/10.5599/jese.565
[21] R. A. Jassim, M. S. Sando, A. M. Farhan, *Baghdad Science Journal* **19** (2022) 347-354. https://doi.org/10.21123/bsj.2022.19.2.0347
[22] N. LeBozec, D. Thierry, D. Persson, C. K. Riener, G. Luckeneder, *Surface and Coatings Technology* **374** (2019) 897-909. https://doi.org/10.1016/j.surfcoat.2019.06.052
[23] M. Ridosic, E. García-Lecina, A. Salicio-Paz, J. Bajat, *Transactions of the IMF* **98** (2020) 114-120. https://doi.org/10.1080/00202967.2020.1748390
[24] O. S. I. Fayomi, O. O. Joseph, I. G. Akande, C. K. Ohiri, K. O. Enechi, N. E. Udoye, *Journal of Alloys and Compounds* **783** (2019) 246-255. https://doi.org/10.1016/j.jallcom.2018.12.312
[25] O. A. Adetayo, O. Jubril, *Fuoye Journal of Engineering and Technology* **4** (2019)145-148. https://doi.org/10.46792/FUOYEJET.V4I1.318
[26] J. G. Thakare, C. Pandey, M. M. Mahapatra, R. S. Mulik, *Metals and Materials International* **27** (2021) 1947-1968. https://doi.org/10.1007/s12540-020-00705-w
[27] V. Kumar, K. Balasubramanian, Progress in Organic Coatings **90** (2016) 54-82. https://doi.org/10.1016/j.porgcoat.2015.09.019
[28] S. G. Croll, Progress in Organic Coatings **148** (2020) 1-14. https://doi.org/10.1016/j.porgcoat.2020.105847
[29] M. Islam, M. R. Azhar, N. Fredj, T. D. Burleigh, O. R. Oloyede, A. A. Almajid, S. I. Shah, *Surface and Coatings Technology* **261** (2015) 141-148. https://doi.org/10.1016/j.surfcoat.2014. 11.044
[30] O. S. I. Fayomi, I. G. Akande, A. P. I. Popoola, Journal of Bio-and Tribo-Corrosion **4** (2018). 1-6. https://doi.org/10.1007/s40735-018-0192-6
[31] A. Buyuksagis, A. T. Baydır, M. Dilek, *Protection of Metals and Physical Chemistry of Surfaces* **57** (2021). 211-221. http://dx.doi.org/10.1134/S2070205120060076
[32] R. Zandi Zand, V. Flexer, M. De Keersmaecker, K. Verbeken, M. Adriaens, *International Journal of Electrochemical Science* **10** (2015) 997-1014. http://hdl.handle.net/1854/LU-5775729
[33] L. Pan, W. Ding, W. Ma, J. Hu, X. Pang, F. Wang, J. Tao, *Materials & Design* **160** (2018) 1106-1116. https://doi.org/10.1016/j.matdes.2018.10.034
T. S. Hamidon, M. H. Hussin, *Progress in Organic Coatings* **140** (2020) 1-12. https://doi.org/10.1016/j.porgcoat.2019.105478
[34] I. G. Akande, O. O. Oluwole, O. S. I. Fayomi, *Defence Technology* **15** (2019) 526-532. https://doi.org/10.1016/j.dt.2018.11.001
[35] C. Y. Ma, D. Q. Zhao, F. F. Xia, H. Xia, T. Williams, H. Y. Xing, *Ceramics International* **46** (2020) 6115-6123. https://doi.org/10.1016/j.ceramint.2019.11.075

[36] M. J. Benoit, I. G. Ogunsanya, S. Winkler, M. J. Worswick, M. A. Wells, C. M. Hansson, *Journal of Materials Engineering and Performance* **30** (2021) 2876-2889. https://doi.org/10.1007/s11665-021-05616-4
[37] K. Brandenburg, D. Hornbach, P. Prevey, N. Jayaraman, *Analysis and Prevention* **21** (2021) 1002–1010. https://doi.org/10.1007/s11668-021-01146-2
[38] A. Singh, G. Singh, V. Chawla, *Journal of the mechanical behavior of biomedical materials* **85** (2018) 20-36. https://doi.org/10.1016/j.jmbbm.2018.05.030
[39] N. Jager, M. Meindlhumer, S. Spor, H. Hruby, J. Julin, A. Stark, R. Daniel, *Acta Materialia* **186** (2020) 545-554. https://doi.org/10.1016/j.actamat.2020.01.026
[40] L. Wang, S. Xing, Z. Shen, H. Liu, C. Jiang, V. Ji, Y. Zhao, *Journal of Materials Science & Technology* **105** (2022) 182-193. https://doi.org/10.1016/j.jmst.2021.08.002
[41] A. Sadeghzadeh-Attar, G. Ayubikia, M. Ehteshamzadeh, *Surface and Coatings Technology* **307** (2016) 837-848. https://doi.org/10.1016/j.surfcoat.2016.10.026
[42] S. Tikale, K. N. Prabhu, *Journal of Materials Science: Materials in Electronics* **32** (2021) 2865-2886. https://doi.org/10.1007/s10854-020-05040-9
[43] K. Alipour, F. Nasirpouri, *Journal of the Electrochemical Society* **166** (2019) D1-D9. https://doi.org/10.1149/2.0191902jes
[44] A. A. Ayoola, O. S. I. Fayomi A. P. I. Popoola, *Defence Technology* **15** (2019) 106-110. https://doi.org/10.1016/j.dt.2018.04.008
[45] M. Sivapragash, P. Kumaradhas, B. S. J. Retnam, X. F. Joseph, U. T. S. Pillai, *Materials & Design* **90** (2016) 713-722. https://doi.org/10.1016/j.matdes.2015.11.027
[46] I. Milosev, G. S. Frankel, *Journal of the Electrochemical Society* **165** (2018) C127-C144. https://doi.org/10.1149/2.0371803jes
[47] X. Li, Y. Feng, B. Liu, D. Yi, X. Yang, W. Zhang, P. Bai, *Journal of Alloys and Compounds* **788** (2019) 485-494. https://doi.org/10.1016/j.jallcom.2019.02.223
[48] J. Wang, H. Yang, H. Huang, J. Ruan, S. Ji, *Journal of Alloys and Compounds* **798** (2019) 576-586. https://doi.org/10.1016/j.jallcom.2019.05.208
[49] T. Han, J. Li, N. Zhao, C. He, *Carbon* **159** (2020) 311-323. https://doi.org/10.1016/j.carbon.2019.12.029